Preparation of boronate affinity controllable-oriented polysaccharides magnetic molecularly imprinted polymer and its application for membrane flux improvement

Qiming Zhang[a,c], Jiajun Hu[b], Chen Yang [a,b], Jixiang Li[a,c,*], Nan Liu[d], Wenshan Guo[e], Chaomeng Dai[f], Liang Wang[g], Yun Tian[h], Huu Hao Ngo[e,*]

[a] Shanghai Advanced Research Institute, Chinese Academy of Sciences, Shanghai 200120, China

[b] Shanghai Key Laboratory of Bio-Energy Crops, School of Life Sciences, Shanghai University, Shanghai 200444, China

[c] University of Chinese Academy of Sciences, Beijing 100049, China

[d] Collaborative Innovation Center of Environmental Pollution Control and Ecological Restoration of Henan Province, Department of Material and Chemical Engineering, Zhengzhou University of Light Industry, Zhengzhou 450001, China

[e] School of Civil and Environmental Engineering, University of Technology Sydney, Sydney, NWS 2007, Australia

[f] College of Civil Engineering, Tongji University, Shanghai, 200092, China

[g] State Key Laboratory of Separation Membrane and Membrane Process, School of Environmental Science and Engineering, Tiangong University, Tianjin 300387, China

[h] Interdisciplinary Research Center for Sustainable Energy Science and Engineering (IRC4SE2), School of Chemical Engineering, Zhengzhou University, Zhengzhou, 450001, China

*Corresponding authors.

E-mail: lijixiang@sari.ac.cn (J.X., Li), HuuHao.Ngo@uts.edu.au (H.H. Ngo).

Abstract:

In this study, researchers successfully developed a novel Magnetic Molecularly Imprinted Polymer of Boronate Affinity Controllable-Oriented Dextran (MMIP-Dextran) to enhance membrane flux by selectively adsorbing polysaccharide-type substances. The structure and components of the MMIP-Dextran were thoroughly investigated using various techniques such as Transmission Electron Microscopy (TEM), Vibrating Sample Magnetometer (VSM), Brunauer-Emmett Teller (BET), Fourier Transform Infrared (FT-IR), and Thermogravimetric Analysis (TGA). Batch experiments were conducted to assess the adsorption performance and mechanisms. Results showed that the MMIP-Dextran exhibited a high adsorption capacity of 31.2 mg g^{-1} and good specific recognition performance (imprinting factor, IF=2.83) for the Dextran template. Furthermore, the MMIP-Dextran had a superior polysaccharide adsorption capacity of 22.10 mg g^{-1} compared to the Non-Imprinted Polymer (NIP) in soluble microbial products (SMPs) derived from a bioreactor, showing a 2.45-fold improvement. Meanwhile, the Specific Filtration Resistance (SFR) tests indicated that the membrane flux improvement by MMIP-Dextran (15.2%) is 2.1 times better than NIP (7.2%). Adsorption kinetics and thermodynamics analyses revealed that the spontaneous adsorption process was predominantly governed by chemically rate-limiting steps. Density Functional Theory (DFT) analysis further revealed that the spatial configuration transformation of the Boric Acid Ligand (BAL) played a crucial role in the adsorption/desorption process. Overall, this study offers a promising approach to promoting the permeate flux of membrane and provides a deeper understanding of the antifouling mechanism using MMIPs.

Keywords: boronate affinity, controllable-oriented polysaccharides, magnetic molecularly imprinted polymer, membrane flux, density functional theory

1. Introduction

Soluble microbial products (SMPs), consisting mainly of proteins and polysaccharides, have been identified as the primary membrane foulants affecting membrane flux in membrane processes, such as membrane bioreactor (MBR), microfiltration (MF), ultrafiltration (UF), nanofiltration (NF), reverse osmosis (RO), etc. [1-4]. Consequently, protein and polysaccharides have garnered significant attention for membrane flux improvement, with

various approaches evaluated for their effectiveness, including membrane modification, pretreatment of feed wastewater, optimization of operational conditions, etc. [5-8]. Among these approaches, the addition of chemicals or absorbents into feed wastewater to remove the SMPs is a promising strategy to improve the membrane flux due to its ease of implementation and effectiveness [9, 10]. For example, Yu et al. demonstrated that the presence of powdered activated carbon and granular activated carbon could improve the membrane flux by adsorbing the organic membrane foulants and enhance UF water treatment performance [11]. Szczuka et al. found that pretreatment of feed wastewater with biological activated carbon could slow down the flux decline of RO membrane [12]. Besides, Zarei et al. reported that adding polyelectrolyte and $KMnO_4$ could significantly diminish the SMPs concentration and improve the membrane flux in MBR [13]. However, the traditional absorbents have a short lifespan and require frequent replacement [14], and overdosing or using larger absorbents can cause abrasion and damage to the membrane [15-18]. Additionally, the use of chemical additives can result in the introduction of extra pollutants and increase the costs of the wastewater treatment process [19].

Compared to the traditional chemicals or absorbents, magnetic molecularly imprinted polymers (MMIPs) have the potential to significantly alleviate membrane fouling. Firstly, MMIPs are known for their specific recognition abilities, making them ideal for the selective adsorption of membrane foulants, resulting in a longer saturation time and less frequent replacement [20-22]. Secondly, the positive magnetic bio-effect is beneficial to the bioreactors, and MMIPs can retain this property along with their specific adsorption abilities. Additionally, the magnetic response properties of MMIPs allow for easy separation and regeneration [23, 24]. While MMIPs have shown exceptional performance in the controllable recognition of micromolecules, their effectiveness in recognizing biomacromolecules has been limited due to high mass transfer resistance and complex structures [25, 26]. However, since membrane foulants are composed of several groups of biomacromolecules, moderate specific recognition for homologous substances is sufficient for effective membrane flux improvement. These advantages of MMIPs have significant implications for future engineering strategies in membrane processes.

Recent studies have shown that polysaccharides are the major contributors to membrane fouling compared to proteins [27, 28]. Also, it has been reported that the boric acid ligand (BAL)

can specially coordinate with the cis-diols on polysaccharides to form cyclic complexes, and can reversibly release it by changing the spatial configuration to facilitate the pH-dependent elution and reuse [29]. Therefore, in this study, a novel MMIP of boronate affinity controllable-oriented dextran (MMIP-Dextran) was developed to selectively adsorb polysaccharides and reduce membrane filtration resistance to improve the membrane flux. The synthesized MMIP-Dextran was characterized using transmission electron microscopy (TEM), thermogravimetric analysis (TGA), Brunauer-Emmett-Teller (BET) surface area analysis, Fourier transform infrared (FT-IR) spectra, and vibrating sample magnetometer (VSM). The adsorption capacity, selectivity, and reusability of the MMIP-Dextran were also investigated. Adsorption isotherms, adsorption thermodynamics, and adsorption kinetics were analyzed to evaluate the adsorption properties, while density functional theory (DFT) was used to determine the adsorption/desorption mechanism. Finally, the MMIP-Dextran was evaluated for its ability to reduce specific filtration resistance (SFR) using practical SMPs from a running MBR. To the best of our knowledge, this is the first report on the use of MMIPs for membrane flux enhancement. The information provided in this study is expected to advance our understanding of the use of MMIPs as effective membrane fouling reducers.

2. Materials and methods

2.1 Materials

The Fe_3O_4 magnetic nanoparticles (MNPs ≤ 30 nm, 98%) used in this study were provided by Aladdin Industrial Corporation (Shanghai, China). Ammonium hydroxide (25%-28%, w/w), glacial acetic acid (Hac), ammonium persulfate (APS), 3-(acrylamido) phenylboronic Acid (AAPBA), N,N'-methylenebisacrylamide (MBA), dextran (MW20000), alginic acid sodium, agarose, tetraethoxysilane, and 3-(trimethoxysilyl) propyl methacrylate (MPS) were sourced from Adamas Reagent Co., Ltd (Shanghai, China). Hydrochloric acid and absolute ethanol were purchased from Sinopharm Chemical Reagent Co., Ltd (Shanghai, China). All the above agents were analytical grade purity. Polyvinylidene fluoride (PVDF) membranes from Shanghai Sinap Membranes Separation Technology Co., Ltd. (Shanghai, China) were used for the SFR tests.

2.2 Preparation of the MMIP-Dextran

The Fe_3O_4@SiO_2 MNPs hybrid carrier was initially prepared using the sol-gel method [30], and then modified by MPS to produce the Fe_3O_4@SiO_2@C=C MNPs hybrid carrier. Lastly, the MMIP-Dextran end product was prepared using AAPBA as the functional monomer, APS as the initiator, MBA as the cross-linking agent, and dextran as the template polysaccharide. The preparation details are as follows:

(1) Preparation of Fe_3O_4@SiO_2@MNPs

Firstly, 5 g of MNPs were dispersed in 1 M HCl solution for 10 min to activate surface hydroxyl, and then were washed 5 times with distilled water. Following, the activated MNPs were dispersed in a mixed solvent of 200 mL ethanol/water (V/V = 4: 1) in a three-necked flask, and then 5 mL $NH_3 \cdot H_2O$ was slowly added under the stirring condition. Finally, 6 mL TEOS was diluted into 20 mL anhydrous ethanol solution and added into the mixture. After a reaction of 8 h at room temperature, the products were collected by an external magnetic field, washed 3 times alternately with deionized water and anhydrous ethanol, and dried under vacuum for 12h at 70 °C.

(2) Preparation of Fe_3O_4@SiO_2@C=C@MNPs

Firstly, 2 mL MPS was evenly dispersed in 240 mL of the aqueous solution containing 10% acetic acid and stirred for 5 h at room temperature. Secondly, 2 g Fe_3O_4@SiO_2@MNPs was added and stirred for 6 h at 60 °C. Next, the products were collected by an external magnetic field, washed 5 times with deionized water, and dried under vacuum for 12 h at 70 °C.

(3) Preparation of MMIP-Dextran

0.25 g dextran and 0.25 g AAPBA were firstly dissolved into a three flask with 250 mL phosphate buffer solution (PBS, pH=9, 0.02 M) and stirred for 60 min at room temperature. Next, 1.25 g Fe_3O_4@SiO_2@C=C MNPs, 1.25 g MBA and 0.5 g APS were added with stirring under nitrogen protection condition. After stirring for 24 h at 60 °C, the products were collected by an external magnetic field, washed three times with deionized water, and washed with PBS (pH = 5.0, 0.02 M). Finally, the products were washed 5 times with deionized water and dried under vacuum for 12 h at 45 °C for subsequent use. The preparation of NIP was the same as MMIP-Dextran without dextran as template molecule.

2.3 Characterization

The morphology of the magnetic microspheres was observed using a transmission electron microscope (TEM, Tecnai G2 F20, USA). Functional groups were characterized by Fourier-transform infrared spectroscopy (FT-IR) using a Nicolet iS5 instrument (Thermal Fisher, USA), the wave number range is 4000-400 cm^{-1}, the scan number is 32 and the resolution is 4 cm^{-1}. Magnetic properties were evaluated using a vibrating sample magnetometer (VSM, 7404, Lakeshore). Surface area tests were performed using Brunauer-Emmett-Teller (BET) analysis with a Micromeritics instrument (USA) under 77 K liquid nitrogen conditions. Thermogravimetric analysis (TGA) was conducted using a PRT-Q600 thermogravimetric analyzer (TA, USA) from 25 °C to 800 °C with a heating rate of 10.0 °C min^{-1} under nitrogen conditions. Filtration resistance was determined using a terminal filtering system at 0.03 MPa (SCM Ultrafiltration Cup, Sinap, China).

2.4 Adsorption experiments

The adsorption of MMIP-Dextran/NIP for the template dextran was systematically evaluated in a dextran (PBS, pH = 9.0, 0.02 M) through equilibrium and kinetic tests. For the equilibrium experiments, 10 mg of MMIP-Dextran/NIP and 10 mL of dextran solution with varying concentrations (0.01 - 0.12 mg mL^{-1}) were mixed in a centrifuge tube and shaken in an orbital shaker (25 °C, 2 h). Following this, the MMIP-Dextran/NIP was separated by a magnet, and the amount of polysaccharides in the supernatant was measured using anthrone-sulfuric acid colorimetry [31]. The equilibrium adsorption amount Q_e (mg g^{-1}) was obtained using the following equation (Eq. 1):

$$Q_e = (C_0 - C_e)\,V / m \quad \text{Eq. (1)}$$

where C_0 (mg mL^{-1}) and C_e (mg mL^{-1}) are the initial and equilibrium polysaccharides concentration; V (mL) is the volume of the initial protein and polysaccharides solution； m (mg) is the mass of the MMIP-Dextran/NIP.

To describe the saturated adsorption data, the Langmuir (Eq. 2), Freundlich (Eq. 3), and Temkin (Eq. 4) isotherm models were employed:

$$\textbf{Langmuir: } \frac{1}{Q_e} = \frac{1}{K_L Q_m C_e} + \frac{1}{Q_m} \quad \text{Eq. (2)}$$

$$\textbf{Freundlich: } Q_e = K_F C_e^{\frac{1}{n_F}} \quad \text{Eq. (3)}$$

Temkin: $Q_e = \alpha \ln \beta + \alpha \ln C_e$ Eq. (4)

where: Q_m (mg g^{-1}) represents the maximum adsorption amount; K_L (mL mg^{-1}) and K_F (mg g^{-1}) are the Langmuir adsorption constant and adsorption strength in the Freundlich isotherm model, respectively; n_F is the adsorption constant; α and β are constants about adsorption enthalpy and adsorbent capacity, respectively.

For the kinetic experiments, 10 mg of MMIP-Dextran/NIP and 10 mL dextran solution (0.8 mg mL^{-1}) were put into a centrifuge tube. Next, the mixtures were shaken in an orbital (25 °C, 2 h). Following this, the dextran concentrations were measured at different times (0 - 240 min). The adsorption amount (Q_t, mg g^{-1}) at different times was obtained by following Eq. (5):

$Q_t = (C_0 - C_t)\,V / m$ Eq. (5)

where C_0 (mg mL^{-1}) and C_t (mg mL^{-1}) are the initial and different times concentrations of dextran in PBS; V (mL) denotes the volume of dextran solution, and m (mg) stands for the mass of the MMIP-Dextran/NIP.

The kinetic experiments data were fitted to pseudo-first-order (Eq. 6), pseudo-second-order (Eq. 7), and Elovich kinetic (Eq. 8) models.

Pseudo-first order: $\ln(Q_e - Q_t) = \ln Q_e - K_1 t$ Eq. (6)

Pseudo-second order: $\frac{t}{Q_t} = \frac{1}{K_2 Q_e^2} + \frac{t}{Q_e}$ Eq. (7)

Elovich: $Q_t = K_e \ln t + A_e$ Eq. (8)

where: Q_t (mg g^{-1}) and Q_e (mg g^{-1}) are captured amounts of dextran in a defined range of adsorption time and the adsorption capacity at equilibrium; K_1 (L min^{-1}), K_2 (g mg^{-1} min^{-1}), and K_e are the rate constants.

Additionally, the thermodynamic parameters, such as Gibbs free energy change (ΔG°), entropy change (ΔS°), and enthalpy change (ΔH°) are calculated using equations (9)-(11):

$$K_D = \frac{Q_e}{C_e} \quad \text{Eq. (9)}$$

$$\ln K_D = -\frac{\triangle H^{\Theta}}{RT} + \frac{\triangle S^{\Theta}}{R} \quad \text{Eq. (10)}$$

$$\triangle G^{\Theta} = \triangle H^{\Theta} - T \triangle S^{\Theta} \quad \text{Eq. (11)}$$

Where Q_e (mg g^{-1}) and C_e (mg L^{-1}) are the equilibrium adsorption capacity on the adsorbent and the equilibrium concentration in the solution, respectively. K_D and R (8.314 J mol^{-1} K^{-1}) are the

equilibrium constant and gas constant, respectively. T (K) is the absolute temperature.

2.5 Selectivity experiments

The selectivity of MMIP-Dextran was evaluated by using sodium alginate and agarose as competitor polysaccharides. To perform the selectivity tests, 10 mg of MMIP-Dextran was added to solutions containing each of the three polysaccharides at a concentration of 0.5 mg mL^{-1}. The mixtures were then shaken at 25 °C for 2 h. After centrifugation (10000 rpm, 10 min), the amount of polysaccharide remaining in the supernatant was measured. The specificity of MMIP-Dextran for dextran was estimated using the imprinting factor (IF) and selectivity factor (α), which were calculated using the following equations, i.e., Eq. (12) and (13):

$$IF = Q_{MIP}/Q_{NIP} \quad \text{Eq. (12)}$$

$$\alpha = IF_{tem}/IF_{ref} \quad \text{Eq. (13)}$$

where Q_{MIP} and Q_{NIP} (mg $g^{-1)}$ are the adsorption capacities of the MMIP-Dextran and NIP, respectively. In Eq. (4), IF_{tem} is the imprinting factor for template polysaccharides (dextran), and IF_{ref} is the reference polysaccharides (sodium alginate or agarose).

2.6 Regeneration tests

The practical application potential of MMIP-Dextran was studied by conducting regeneration tests for five cycles. Initially, 100 mg of MMIP-Dextran was added into 100 mL dextran solution (0.5 mg mL^{-1}, pH = 9) and shaken at 25 °C for 2 h. The content of polysaccharides in the supernatant after centrifugation (10000 rpm, 10 min) was measured. For the next cycle reuse, the separated MMIP-Dextran was washed several times with PBS (pH = 5.0, 0.02 M) and water for regeneration.

2.7 DFT calculations

All DFT calculations were performed using the Gamma-centered Monkhorst-Pack scheme with the Vienna Ab initio Simulation Package (VASP). The Perdew-Burke-Ernzerhof (PBE) functional within the generalized-gradient-approximation (GGA) was used to describe the exchange-correlation interaction. The static computations and structure optimization were conducted using a cutoff energy of 400 eV. Post-processing of the VASP computational data was carried out using the VASPKIT code.

2.8 Evaluation of membrane filtration resistance

The content of SMPs is typically represented by the total amount of protein and polysaccharides.

SMPs were extracted using a modified thermal method [32]. To determine the protein and polysaccharides contents of the SMPs, 0.15 g of MMIP-Dextran or NIP was added to a closed conical flask containing 150 mL of the extracted SMPs solution. The batch adsorption experiments were conducted by following the same procedures as described earlier. The protein content was quantified using the bicinchoninic acid assay (BCA) method. Furthermore, as shown in Fig. 1, the supernatant was subjected to membrane filter resistance analysis using a terminal filtration device. The ultrafiltration cup of the terminal filtration device had a volume of 300 mL, and a constant pressure of 0.03 MPa was maintained during the experiment. PVDF membrane was used for ultrafiltration, and the membrane area was 0.0032 m^2. Under constant pressure, the filtrate passing through the PVDF membrane was collected in a beaker on a balance, and the weight of the filtrate was recorded. All the tests were repeated in triplicate. The filter resistance R (m^{-1}) was calculated using Equation (14):

$$R = \Delta P / (J \times \eta) \quad \text{Eq. (14)}$$

where ΔP (Pa) is the constant pressure in the experiment, J (m^3 (m^2•s)$^{-1}$) is the amount of material passing through the unit membrane area per unit time, and η (kg (m•s^2)$^{-1}$) is the viscosity.

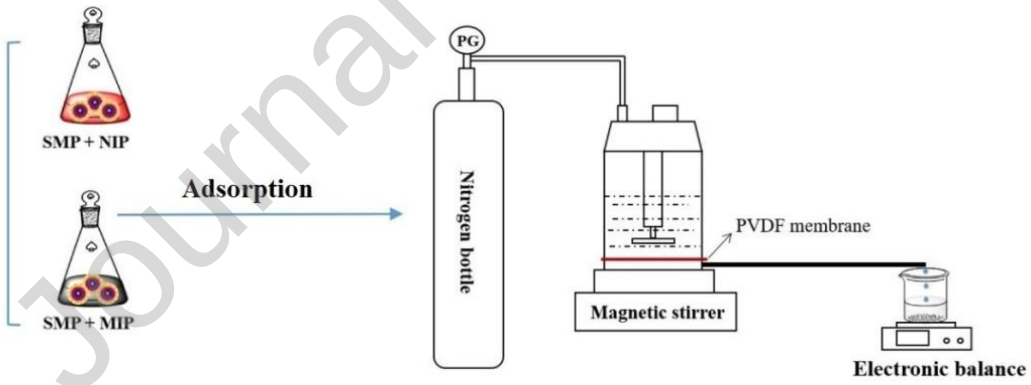

Fig. 1: Terminal filtering device

3. Results and discussion

3.1 The preparation of MMIP-Dextran

The synthesis of MMIP-Dextran is illustrated in Fig. 2. Initially, Fe_3O_4 MNPs were coated with SiO_2 to obtain Fe_3O_4@SiO_2 hybrid carriers using the sol-gel method. The SiO_2 layer not only prevented the oxidation of Fe_3O_4 but also provided a biocompatible and hydrophilic surface [33]. Next, a C=C bond was grafted onto the surface of Fe_3O_4@SiO_2 MNPs to facilitate the

introduction of BAL. Subsequently, BAL was introduced to enhance the adsorption capacity through the covalent bond between BAL and the 1,2-cis-diol group in dextran. Dextran was then imprinted using specific recognition of BAL and the 1,2-cis-diol group. Finally, the products were vigorously washed multiple times under acidic conditions to completely remove the template dextran. In addition, the ratio of AAPBA to MBA was optimized to improve the adsorption capacity of MMIP-Dextran (see section 3.2).

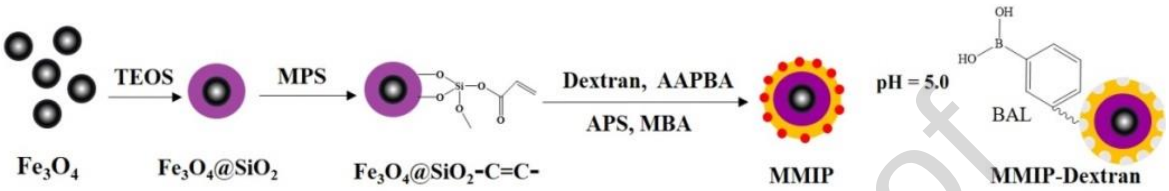

Fig. 2: The preparation scheme of MMIP-Dextran

3.2 Optimization of the ratio of functional monomer to crosslinker

The adsorption capacity of polymers prepared with different ratios of functional monomers (i.e., AAPBA) and cross-linking agents (i.e., MBA) may be different due to the following reasons: Firstly, the imprinted surface shell is too thick. When increasing the proportion of APBA, the specific recognition cavities are buried due to the dense distribution of boron elements and excessive functional monomers, and the imprinting performance is significantly depressed. Secondly, the insufficient polymerization reaction may decrease the adsorption capacity. Too few functional monomers cannot fully polymerize with template molecules, and inadequate specific recognition sites are formed. The number of imprinted sites decreases, the adsorption capacity decreases, and the non-specific recognition sites will also be blocked. Therefore, optimizing the ratio of AAPBA to MBA is critical to improving the adsorption capacity of polymers.

The molar ratio of AAPBA to EGDMA in the preparation process was optimized according to the adsorption capacity Q (mg g^{-1}) of the prepared polymer for dextran (Fig. 3). The adsorption conditions are as follows: 0.05g polymer (MMIP-Dextran/NIP), 50 mL Dextran solution (PBS, pH = 9.0, 100 mg L^{-1}), 200 rpm, 25 ºC water bath shock adsorption conditions for 2 h. By testing the functional monomers with different molar ratios and cross-linking agents, it is found that the adsorption capacity Q of MIPs-Dextran increases first and then decreases with the increase of MBA dosage. When the APBA/MBA molar ratio is 1:5, the adsorption capacity reaches the maximum of 31.19 mg g^{-1}, and the IF calculated by Eq. (12) is 2.83.

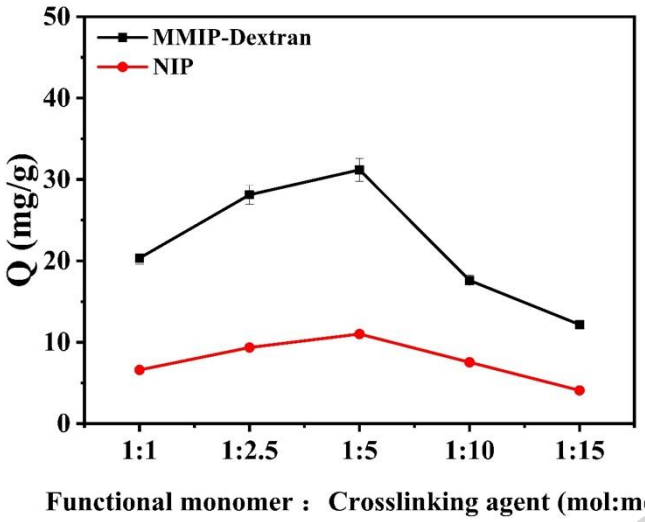

Fig. 3: Effect of the molar ratio of functional monomer (i.e., AAPBA) to cross-linking agents (i.e., MBA) on the adsorption capacity

3.3 Characterization of MMIP-Dextran

The morphology and characteristics of the carriers and MMIP-Dextran/NIP were analyzed using TEM. Fig. 4a shows that the Fe_3O_4 MNPs have a uniform particle size and good dispersion. The particle size of Fe_3O_4@SiO_2 MNPs slightly increased (Fig. 4b), which can be attributed to the successful coating of silica [34]. Also, it can be seen that the silica covers the agglomerates of Fe_3O_4 MNPs, not each single Fe_3O_4 MNP, probably owing to their magnetism. In Fig. 4c, it can be observed that the particle size of MMIP-Dextran also slightly increased. The thickness of the imprinting shell was estimated to be around 5-10 nm, which suggests that the thin imprinted-layer is conducive to rapid specific recognition and elution of the template molecules. Furthermore, Fig. 4d demonstrates that MMIP-Dextran has better dispersion capabilities than NIP, which is related to the spatial effect of dextran. Both MMIP-Dextran and NIP possess typical core-shell structures.

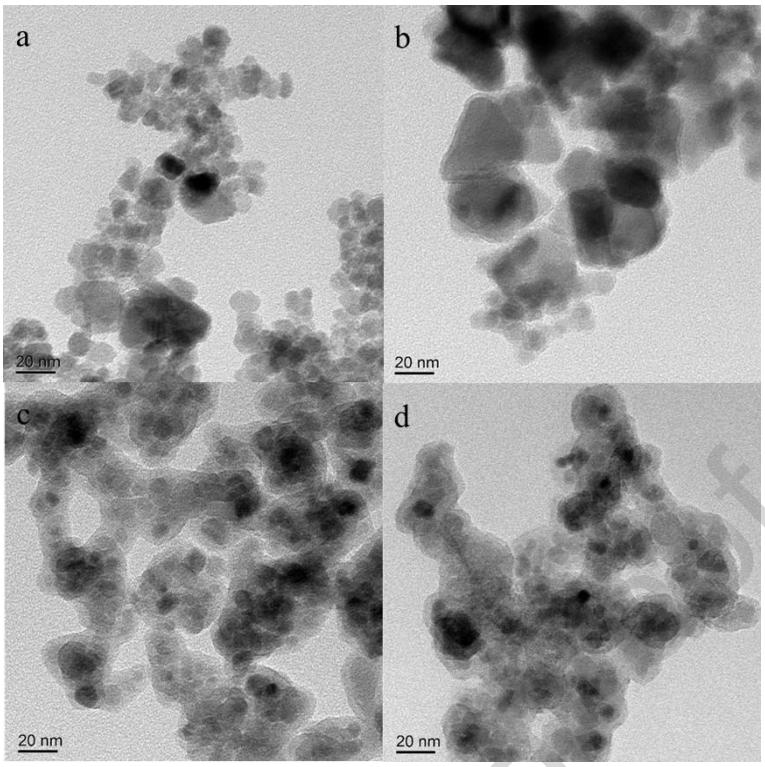

Fig. 4: TEM images of (a) Fe_3O_4, (b) Fe_3O_4@SiO_2, (c) MMIP-Dextran and (d) NIP

The carriers and MMIP-Dextran were characterized using FT-IR spectroscopy to confirm the presence of SiO_2, C=C grafts, and BAL (Fig. 5a). The peaks at 1630 cm^{-1} and 1404 cm^{-1} indicate the stretching vibrations of asymmetric COO- and symmetric COO- respectively. Additionally, the peak at 582 cm^{-1} is attributed to Fe-O [35], while the peaks at 796 cm^{-1} and 1083 cm^{-1} correspond to the bending vibration and stretching vibration of Si-O-Si bonds [36], confirming the successful coating of inorganic silica on the Fe_3O_4 surface. Treatment with MPS results in a new peak at 1698 cm^{-1} in the spectrum of Fe_3O_4@SiO_2-C=C, indicating the presence of the C=C bond. The peaks at 1452 cm^{-1} and 1325 cm^{-1} correspond to the B-O stretching, confirming the successful modification of BAL on the MMIP-Dextran [37].

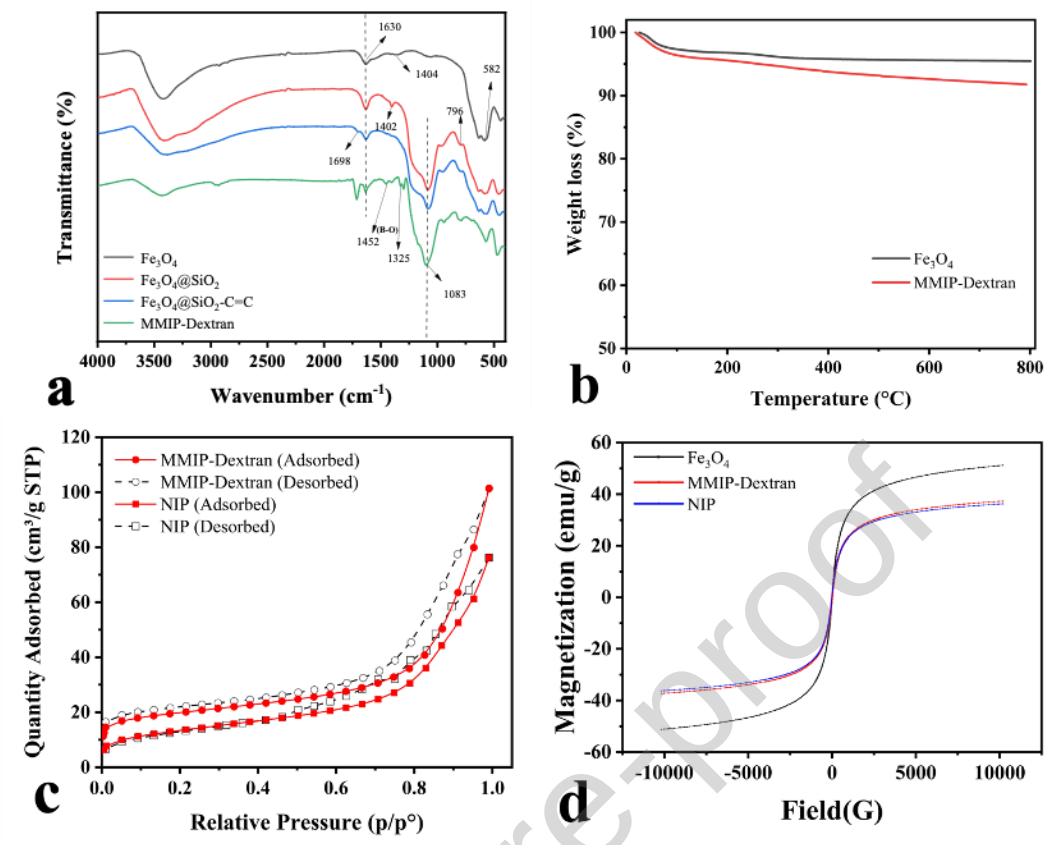

Fig. 5: FT-IR spectra for Fe_3O_4, Fe_3O_4@SiO_2, Fe_3O_4@SiO_2-C=C and MMIP-Dextran (a), TGA curves of Fe_3O_4, MMIP-Dextran and NIP (b), N_2 physisorption isotherms (77.30 K) obtained for MMIP-Dextran and NIP (c), Magnetization loops of Fe_3O_4, MMIP-Dextran and NIP (d)

TGA was used to study the thermostability and solid content of Fe_3O_4 and MMIP-Dextran. The curves in Fig. 5b show no significant weight loss below 200 ℃, indicating good thermal stability of MMIP-Dextran. The weight loss of Fe_3O_4 above 200 ℃ may be due to thermal decomposition of surface impurities, while the weight loss of MMIP-Dextran is attributed to the decomposition of polymer shells [38]. These results are consistent with the TEM images.

The BET specific surface areas of MMIP-Dextran and NIP were measured using the N_2 adsorption-desorption method. Both exhibit an adsorption hysteresis loop belonging to isotherm IV [39], indicating the presence of mesopores (2-50 nm) in the polymers. As shown in Table 1, the S_{BET}, V_p and D_{pBJH} values of MMIP-Dextran are 43%, 23%, and 38% higher than those of NIP, respectively. Furthermore, the S_{BET} value of MMIP-Dextran is 3.2 times larger than the analogous materials noted by Cao et al. [40], indicating that MMIP-Dextran may have better absorption capacity. The magnetic properties of Fe_3O_4, MMIP-Dextran and NIP were evaluated

using VSM to measure the magnetic hysteresis loops. As depicted in Fig. 5d, all hysteresis loops showed centrosymmetric behavior with respect to the origin. The saturation magnetization values of Fe_3O_4, MMIP-Dextran and NIP were 51.23 emu g^{-1}, 37.34 emu g^{-1} and 36.30 emu g^{-1}, respectively. This indicates that the high saturation magnetization of MMIP-Dextran (37.34 emu g^{-1}) facilitates rapid and efficient magnetic separation, and demonstrates promising potential for future engineering applications [41]. In summary, this study successfully prepared a core-shell structure of MMIP-Dextran with a controllable-oriented polysaccharide-imprinted shell.

Table 1: BET parameters of MMIP-Dextran and NIP

Samples	S_{BET} **(m^2 g^{-1})**	V_p **(cm^3 g^{-1})**	$D_{p\ BJH}$ **(nm)**	**References**
MMIP-Dextran	65.33	0.1418	15.06	This work
NIP	45.51	0.1136	11.34	This work
MMIP	20.42	0.1217	30.72	[33]

S_{BET}: BET surface area; V_p: pore volume; $D_{p\ BJH}$: BJH pore diameter.

3.4 Adsorption properties analysis

3.4.1 The effect of pH on the binding ability

As it is well established, the boronate affinity is pH-dependent [42], and therefore, we evaluated the effect of pH on the binding ability, which is presented in Fig. 6. It can be seen that both MMIP-Dextran and NIP exhibit an ascending-then-descending trend in adsorption capacity as pH increases in the range of 7.0-10.0, with the highest values occurring around pH 9. This phenomenon can be attributed to the diverse covalent interactions between boronic acid ligands (BAL) and 1,2-cis-diol groups, as shown in Fig. 7. At pH values above the pKa of the boronic acid (8.0-9.0), BAL adopts a tetragonal boronate anion configuration (sp3), which reacts with 1,2-cis-diols to form five/six-membered cyclic complexes, leading to high adsorption capacity of dextran by MMIP-Dextran. However, when the pH is increased further to 9 and above, electrostatic repulsion between adsorbents and adsorbates becomes dominant, resulting in a decline in adsorption capacity. Conversely, under acidic conditions, BAL adopts

a trigonal configuration (sp2) and the boronic acid–cis-diol complex is greatly reduced, leading to a lower capacity to adsorb dextran [43]. Nonetheless, MMIP-Dextran exhibits a higher ability to adsorb dextran than NIP at any pH level. Based on these findings, subsequent batch adsorption experiments were carried out under alkaline conditions (pH=9.0).

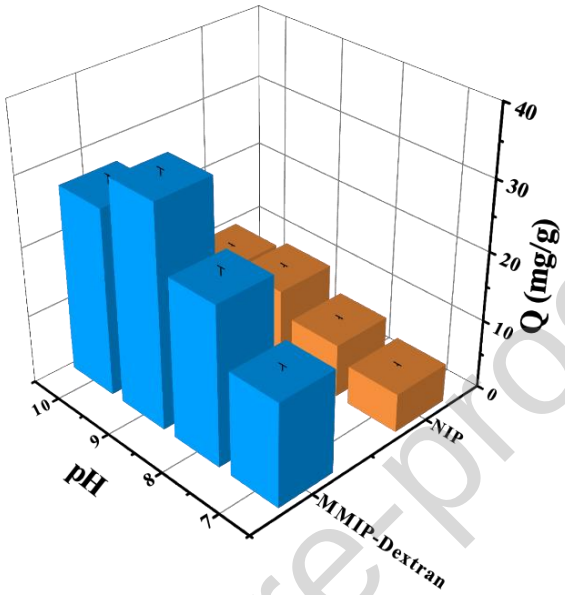

Fig. 6: The adsorption of dextran on MMIP-Dextran and NIP under different pH conditions

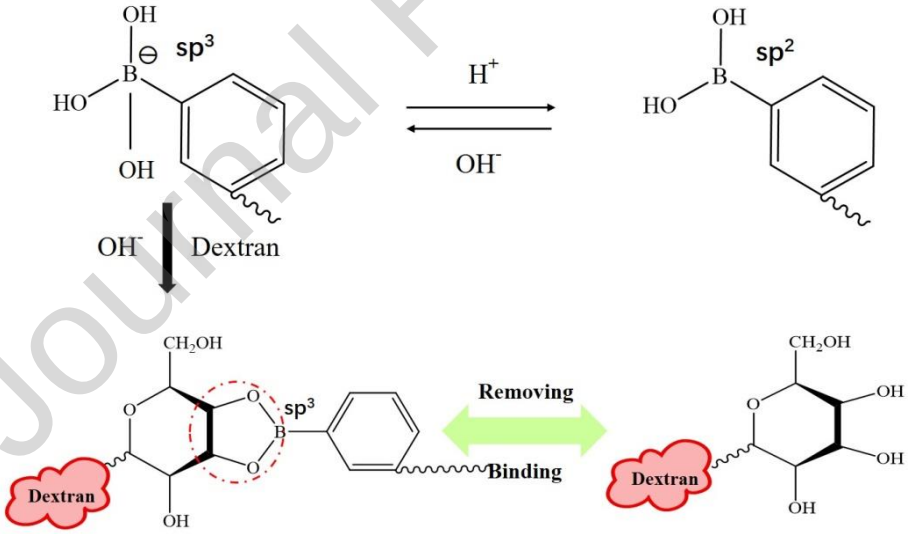

Fig. 7: The interaction between BAL and dextran

In conclusion, the results of this study indicate that the adsorption of dextran by MMIP-Dextran is significantly affected by the solution pH and is consistent with the pKa value of the boronic acid. Therefore, it may be possible to enhance the adsorption affinity by controlling the pKa values. Ongoing work is focused on exploring this possibility and will be reported in the near future.

3.4.2 Adsorption kinetics

The adsorption kinetics curves of MMIP-Dextran and NIP at 25 °C and pH 9 are presented in Fig. 8a. In addition, the experimental data were fitted to pseudo-first-order (Eq. 6), pseudo-second-order (Eq. 7), and Elovich kinetic (Eq. 8) models. The kinetics parameters and linear regression values are summarized in Table 2 below.

As shown in Fig. 8a, both MMIP-Dextran and NIP exhibit fast initial adsorption within the first 40 minutes due to the high initial concentration gradient of dextran and numerous vacant imprinted sites. Thereafter, the adsorption rate slows down and reaches equilibrium. The equilibrium adsorption capacity (Q_e) of MMIP-Dextran is 31.2 mg g^{-1}, which is significantly higher than that of NIP (11.0 mg g^{-1}), owing to the numerous BAL binding sites on MMIP-Dextran.

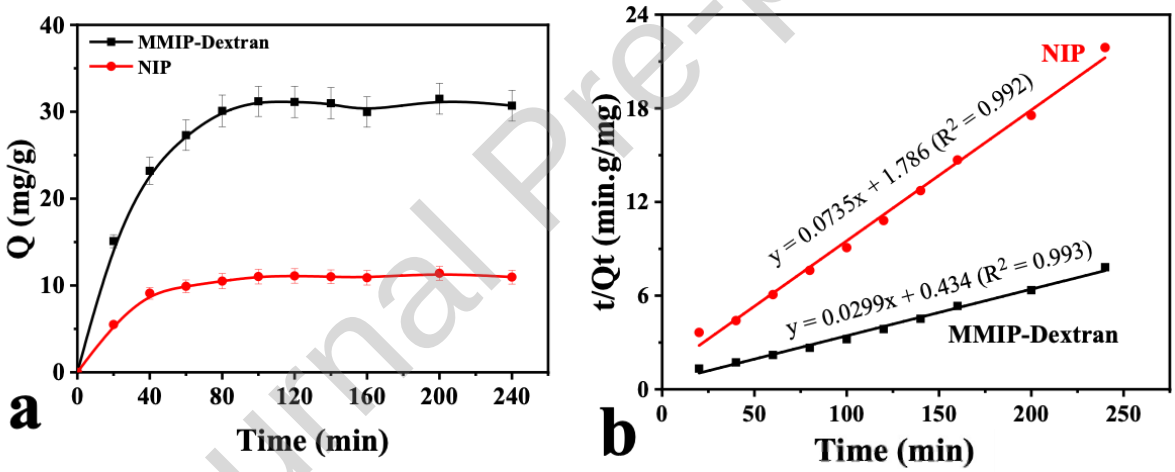

Fig. 8: The adsorption kinetic curves of Dextran on MMIP-Dextran and NIP (a); the pseudo-second-order adsorption kinetics curves of Dextran on MMIP-Dextran and NIP (b)

As shown in Table 2, the results indicate that the adsorption of dextran on MMIP-Dextran and NIP follows the pseudo-second-order model. Moreover, the Q_e value obtained from the pseudo-second-order kinetic model (33.44 mg g^{-1}) is much closer to the experimental data (31.2 mg g^{-1}) than the other models. These findings suggest that the chemical interaction between dextran and the BAL binding site on MMIP-Dextran is probably the rate-limiting step and dominates the adsorption of dextran on the adsorbents [44]. The absence of interior and exterior diffusion resistance is probably due to the complete shaking of the solution, leading to a low exterior diffusion resistance and a high adsorption specific surface area. This phenomenon

allows dextran to spread fully on the adsorbents, providing more opportunities for BAL to combine with the 1, 2-cis-diol group and achieve high adsorption efficiency. These results further support the idea that a large surface area of the adsorbent is beneficial for adsorption [45].

Table 2: Kinetic parameters obtained from adsorption of dextran on MMIP-Dextran and NIP

Models	**MMIP-Dextran**		**NIP**	
Pseudo-first-order kinetic model	k_1	0.016	k_1	0.0142
	Q_e	23.831	Q_e	7.512
	R^2	0.925	R^2	0.909
Pseudo-second-order kinetic model	K_2	0.009	K_2	0.003
	Q_e	33.44	Q_e	13.61
	R^2	0.993	R^2	0.992
Elovich kinetic model	K_3	6.111	K_3	2.049
	A_e	0.406	A_e	0.847
	R^2	0.804	R^2	0.794

3.4.3 Adsorption isotherms

The adsorption isotherms of MMIP-Dextran and NIP were determined using a series of dextran solutions, and the results are shown in Fig. 9a. The Q_e values of both adsorbents initially increase sharply with increasing dextran concentration, then plateau, and finally reach saturation. The saturated adsorption capacities of MMIP-Dextran and NIP are 31.2 mg g^{-1} and 11.0 mg g^{-1}, respectively. To describe the saturated adsorption data, the Langmuir (Eq. 2), Freundlich (Eq. 3), and Temkin (Eq. 4) isotherm models were employed.

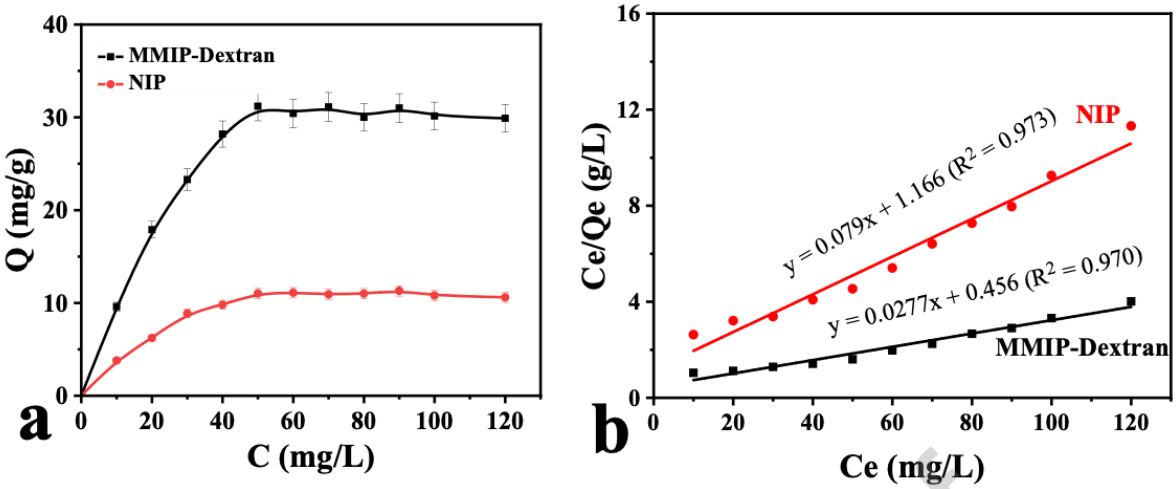

Fig. 9: The adsorption isotherm data of Dextran on MMIP-Dextran and NIP (a); the Langmuir adsorption sotherms fitting curves of Dextran on MMIP-Dextran and NIP (b)

Table 3: Parameters of the isotherms from adsorption of Dextran on MMIP-Dextran and NIP

Isotherm models	Parameter	MMIP-Dextran	NIP
Langmuir Isotherm	Q_m	35.714	12.723
	K	0.061	0.067
	R^2	0.970	0.973
	R_L	0.12-0.62	0.11-0.59
Freundlich Isotherm	K_F	4.691	1.880
	n_F	2.312	2.460
	R^2	0.804	0.814
Temkin Isotherm	α	8.494	2.953
	β	0.464	0.519
	R^2	0.842	0.844

The parameters of the isotherm experiment are shown in Table 3. The Langmuir model provides the best fit to the adsorption data, and the Q_m value (35.7 mg g^{-1}) in the Langmuir model is much closer to the experimental adsorption capacity (31.2 mg g^{-1}). These results indicate that the adsorption process between MMIP-Dextran and dextran is a monolayer process that occurs on a homogeneous surface with uniform energies and BAL active sites. Moreover, the separation factor constant (R_L) is used to determine the favorability of MMIP-Dextran/NIP towards dextran [46]. The obtained R_L values for both MMIP-Dextran and NIP fall between 0 and 1, indicating that the adsorption of dextran on MMIP-Dextran/NIP is favorable. The R_L

value of MMIP-Dextran is higher than that of NIP, indicating that the adsorption of dextran on MMIP-Dextran is more favorable than on NIP.

3.4.4 Adsorption thermodynamics

The adsorption properties of MMIP-Dextran and NIP at different temperatures are presented in Table 4. It is observed that both adsorbents show higher adsorption capacity at higher temperatures, indicating an endothermic process between dextran and MMIP-Dextran. Additionally, the thermodynamic parameters, such as Gibbs free energy change (ΔG°), entropy change (ΔS°), and enthalpy change (ΔH°) are calculated using equations (9)-(11).

The negative values of $\triangle G^{\Theta}$ indicate that the adsorption process of dextran on MMIP-Dextran is spontaneous, which is advantageous in adsorbing polysaccharide-type membrane fouling substances in complex environments. The decrease in $\triangle G^{\Theta}$ with an increase in temperature suggests that higher temperatures favor the adsorption process. Moreover, the positive values of $\triangle H^{\Theta}$ and $\triangle S^{\Theta}$ indicate that the adsorption of dextran on MMIP-Dextran is an endothermic process and an increase in the randomness at the adsorbent/adsorbate interfaces.

Table 4: Effect of temperature on the adsorption capacity

Polymers	T (°C)	Q_e (mg g^{-1})	K_D	ΔH^{Θ} (kJ mol^{-1})	ΔS^{Θ} (J mol^{-1} K^{-1})	ΔG^{Θ} (kJ mol^{-1})
MMIP-Dextran	25	31.0	1512	25.97	90.54	-1.024
	35	34.1	2125			-1.930
	45	37.3	2937			-2.835
NIP	25	11.0	282.7	4.51	62.01	-13.98
	35	11.5	299.7			-14.60
	45	12.8	344.1			-15.23

3.4.5 Specific capture capacity

To evaluate the adsorption selectivity and capacity of MMIP-Dextran for polysaccharides, several tests were conducted using model membrane foulants. The data for the imprinting factor (IF) and the selection factor (α) are displayed in Table 5. The highest adsorption amount and IF of MMIP-Dextran for dextran suggest that the BAL binding sites on the surface of MMIP-

Dextran match the target dextran, enabling specific recognition covalent interaction. The capacity of NIP to adsorb the three homologous substances is virtually the same, but much lower than MMIP-Dextran. It can be concluded that electrostatic interaction contributes less to the adsorption capacity than the specific recognition covalent interaction of the imprinting cavity. On the other hand, α suggests that the polymers can adsorb different polysaccharides specifically and non-specifically. As a result, the adsorption amount and IF of MMIP-Dextran for agarose are higher than for sodium alginate. It is evident that agarose has a lower α than sodium alginate, likely due to its larger molecular weight and the larger number of 1, 2-cis-diol groups, providing more opportunities to bond with BAL. In summary, MMIP-Dextran exhibits excellent selectivity for selectively adsorbing the template molecules of dextran. The above results indicate that the MMIP-Dextran has significant potential for reducing polysaccharide-type membrane filtration resistance.

Table.5: Comparison of MMIP-Dextran to different polysaccharides

Polysaccharides	**Q_e (mg g^{-1})**		**IF**	**α**
	MMIP-Dextran	**NIP**		
Dextran	31.2	11.0	2.84	/
Agarose	19.2	7.0	2.74	1.04
Sodium Alginate	10.4	8.2	1.27	2.24

3.4.6 Reusability and stability

The reusability and stability of MMIP-Dextran are important factors for its practical application. The adsorption and desorption experiments were repeated five times to assess the reusability of MMIP-Dextran, and the results are shown in Fig.10. It is noteworthy that the adsorption capacity remains at 92.68% after five cycles, indicating its good reusability. The slight decrease in adsorption capacity may be attributed to the blocking or damage of some binding sites, as reported in previous studies [47]. Moreover, after five cycles of adsorption-desorption, MMIP-Dextran still exhibits excellent magnetic responsiveness, facilitating its rapid separation. The use of SiO_2 coating under an acid elution environment can effectively prevent the leakage of Fe_3O_4 MNPs. These findings indicate that the desorption and reuse of MMIP-Dextran are feasible and efficient, making it a promising candidate for promoting membrane flux.

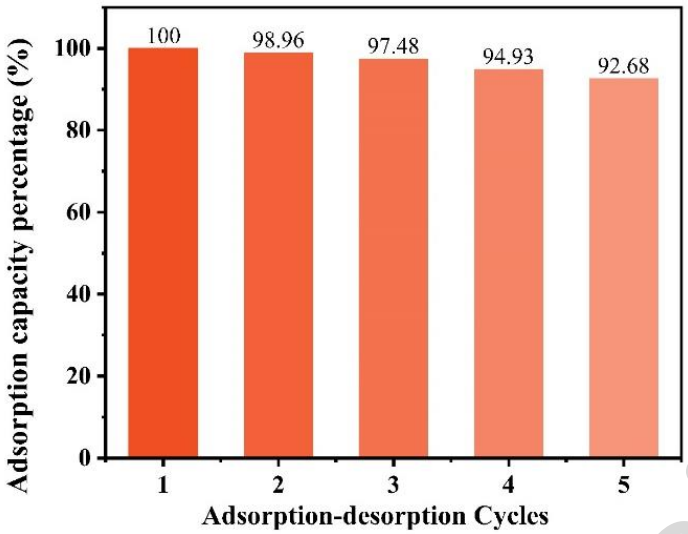

Fig. 10: Reusability of MMIP-Dextran

3.5 The adsorption/desorption mechanism by DFT

The mechanism of adsorption and desorption between MMIP-Dextran and dextran was elucidated by DFT calculations, and the results are depicted in Fig. 11. During the adsorption process, it can be inferred that under alkaline conditions, the boron atom in BAL is firstly transformed from a trigonal configuration (sp2) to a tetragonal anion (sp3). Subsequently, the BAL with boron-sp3 atom can interact with 1,2-cis-diols to form five/six cyclic complexes, ultimately leading to the successful attachment of dextran on the surface of MMIP-Dextran. These results suggest that the coordination process, in which a five/six cyclic complex is formed by the conformation conversions of boron atom, is the rate-limiting step of the adsorption process. The negative relative free energy data of the INT1 and INT2 states support this hypothesis.

For the desorption process, it is assumed that under acidic conditions, the boron atom in BAL converts back to a trigonal configuration (sp2) from a tetragonal anion (sp3), and the BAL with boron-sp2 atom promotes the desorption of dextran from MMIP-Dextran. The negative energy of state INT3 confirms the thermodynamic feasibility of the transformation of the BAL geometric configuration. Subsequently, the boronic acid-cis-diol five/six complex significantly dissolves, leading to the desorption of dextran from MMIP-Dextran. Moreover, the positive energy data of the INT4 state implies that a complete desorption may only occur under external energy, such as violent shocks. The above results are consistent with the adsorption thermodynamics results.

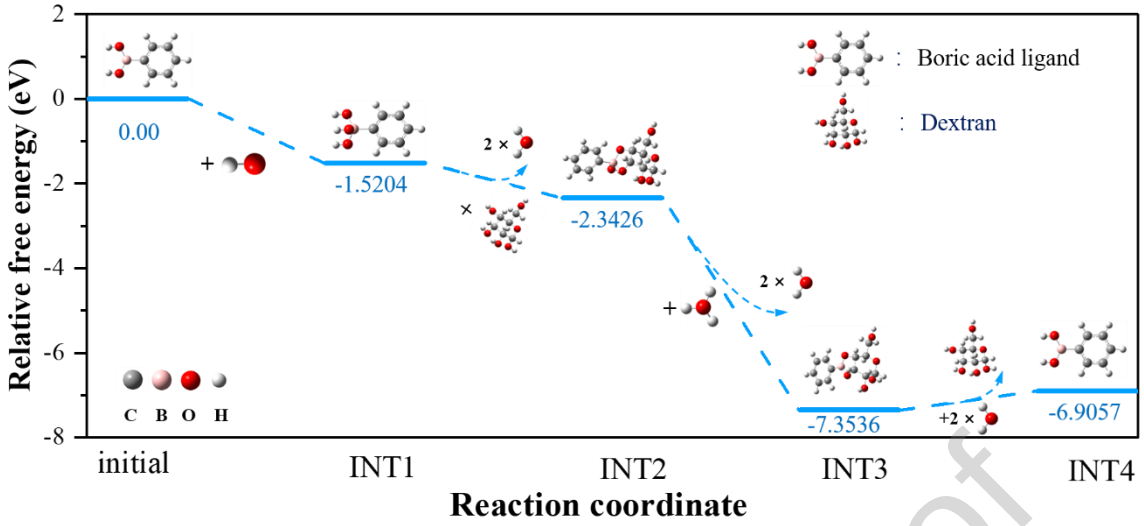

Fig. 11: DFT calculations of energy states for adsorption/desorption process by MMIP-Dextran to dextran

3.6 Evaluation of membrane permeate flux

In order to assess the practical application potential and viability of the polymers, adsorption experiments were conducted using SMPs as membrane foulants. As shown in Fig. 12a, the adsorption capacities of MMIP-Dextran and NIP for polysaccharides were found to be 22.10 mg g^{-1} and 9.02 mg g^{-1}, respectively. Notably, the adsorption capacity of MMIP-Dextran was 2.45 times higher than that of NIP, while both showed similar and low capacities for protein adsorption. These results indicate that MMIP-Dextran can selectively adsorb polysaccharides and non-specifically adsorb a few biomacromolecules. This suggests that the bonding between BAL and 1,2-cis-diol group enables MMIP-Dextran to effectively recognize dextran and its homologous substances.

An evaluation of membrane filtration resistance was conducted using a terminal filtration device, and the results are presented in Fig. 12b. Compared to the initial SMPs, the control group showed a slight increase in filter resistance, which could be attributed to the residual microorganisms' metabolism in the SMPs. However, the filter resistances of the MMIP-Dextran and NIP groups decreased by 15.2% and 7.2%, respectively. Accordingly, it means the membrane flux improvement by MMIP-Dextran group is 2.1 times better than NIP. These results, in conjunction with the SFR results, indicate that the MMIP-Dextran can selectively adsorb polysaccharide-type substances and effectively reduce membrane filtration resistance. Therefore, this study proposes a promising strategy for promoting the membrane flux using

MMIPs and is expected to be applied to the polysaccharide-type membrane fouling in membrane processes.

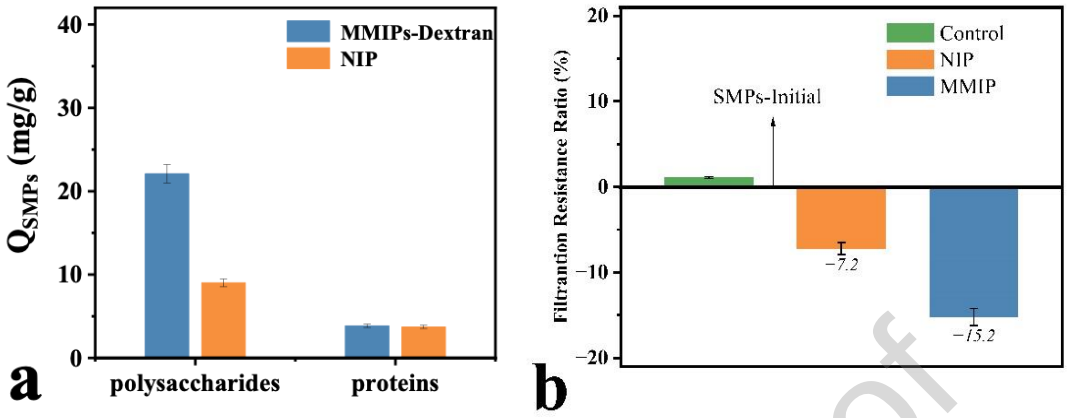

Fig. 12: The adsorption capacity of SMPs on MMIP-Dextran and NIP (a) and the effects of MMIP-Dextran and NIP on filtration resistances (b)

4. Conclusion

This study successfully developed, characterized, and applied a novel MMIP-Dextran to enhance the membrane flux. The MMIP-Dextran exhibits a typical core-shell structure with a rough surface, high saturation magnetization, good thermal stability, and great dispersion. Additionally, it possesses specific recognition to the template and a large specific surface area. The MMIP-Dextran demonstrates excellent recognition towards dextran and its homologous substances, resulting in a significant reduction in membrane filtration resistance. The adsorption isotherm of MMIP-Dextran and dextran best follows the Langmuir model with the separation constant falling between 0 and 1, indicating favorable monolayer adsorption. The spontaneous and endothermic adsorption fits well with the pseudo-second-order model and Langmuir Isotherm. DFT calculations support that the spatial configuration of BAL plays a vital role in the adsorption/desorption process. Additionally, the MMIP-Dextran maintains a high adsorption capacity and excellent magnetic response even after several adsorption-desorption cycles. These results demonstrate that the MMIP-Dextran is a promising solution for minimizing polysaccharide-type membrane fouling and will significantly benefit membrane flux.

Acknowledgements

The authors appreciate the support of the National Natural Science Foundation of China

(51878646, 22131004 , 42077175 and 52270164) and the National Key R&D Program of China (2021YFE0192600 and 2019YFE0114900).

Reference

[1] Y. Zhang, Q. Fu, Algal fouling of microfiltration and ultrafiltration membranes and control strategies: A review, Sep. Purif. Technol. 203 (2018) 193-208. https://doi.org/10.1016/j.seppur.2018.04.040.

[2] J. Kulandaivelu, S. Shrestha, W. Khan, J. Dwyer, A. Steward, L. Bell, P. McPhee, P. Smith, S. Hu, Z. Yuan, G. Jiang, Full-scale investigation of ferrous dosing in sewers and a wastewater treatment plant for multiple benefits, Chemosphere 250 (2020) 126221. https://doi.org/10.1016/j.chemosphere.2020.126221.

[3] W. Guo, H.-H. Ngo, J. Li, A mini-review on membrane fouling, Bioresour. Technol. 122 (2012) 27-34. https://doi.org/10.1016/j.biortech.2012.04.089.

[4] K. Kimura, K. Kume, Irreversible fouling in hollow-fiber PVDF MF/UF membranes filtering surface water: Effects of precoagulation and identification of the foulant, J. Membr. Sci. 602 (2020). https://doi.org/10.1016/j.memsci.2020.117975.

[5] K. Gupta, S. Chellam, Revealing the mechanisms of irreversible fouling during microfiltration-The role of feedwater composition, J. Environ. Chem. Eng. 10(2) (2022). https://doi.org/10.1016/j.jece.2022.107362.

[6] A. Robles, M.V. Ruano, A. Charfi, G. Lesage, M. Heran, J. Harmand, A. Seco, J.P. Steyer, D.J. Batstone, J. Kim, J. Ferrer, A review on anaerobic membrane bioreactors (AnMBRs) focused on modelling and control aspects, Bioresour. Technol. 270 (2018) 612-626. https://doi.org/10.1016/j.biortech.2018.09.049.

[7] X. Du, Y. Shi, V. Jegatheesan, I.U. Haq, A Review on the Mechanism, Impacts and Control Methods of Membrane Fouling in MBR System, Membranes-Basel 10 (2) (2020) 24. https://doi.org/10.3390/membranes10020024.

[8] I. Koyuncu, B.Y. Gul, M.S. Esmaeili, E. Pekgenc, O.O. Teber, G. Tuncay, H. Karimi, S. Parvaz, A. Maleki, V. Vatanpour, Modification of PVDF membranes by incorporation Fe_3O_4@Xanthan gum to improve anti-fouling, anti-bacterial, and separation performance, J. Environ. Chem. Eng. 10(3) (2022). https://doi.org/10.1016/j.jece.2022.107784.

[9] M.E. Wang, Q.H. Cen, R. Zeng, Y.D. Huang, Y.L. Liu, S.J. Xia, Performance of a hybrid process integrating PAC adsorption with ceramic membrane ultrafiltration for drinking water treatment, J. Environ. Chem. Eng. 10(5) (2022). https://doi.org/10.1016/j.jece.2022.108427.

[10] J. Xiong, S. Yu, Y. Hu, Y. Yang, X.C. Wang, Applying a dynamic membrane filtration (DMF) process for domestic wastewater preconcentration: Organics recovery and bioenergy production potential analysis, Sci. Total Environ. 680 (2019) 35-43. https://doi.org/10.1016/j.scitotenv.2019.05.080.

[11] Yu. S, Wang. J, Zhao. Z, Cai. W, Simultaneous coupling of fluidized granular activated carbon (GAC) and powdered activated carbon (PAC) with ultrafiltration process: A promising synergistic alternative for water treatment. Sep. Purif. Technol. 282 (2022), 120085. https://doi.org/10.1016/j.seppur.2021.120085.

[12] Szczuka. A, Berglund-brown. J.P, Chen. H.K, Quay A.N, Mitch. W.A, Evaluation of a Pilot Anaerobic Secondary Effluent for Potable Reuse: Impact of Different Disinfection Schemes on Organic Fouling of RO Membranes and DBP Formation. Environ. Sci. Technol. 53 (6) (2019), 3166-3176. https://doi.org/10.1021/acs.est.8b05473

[13] A. Zarei-Baygi, M. Moslemi, S.H. Mirzaei, The combination of $KMnO_4$ oxidation and polymeric flocculation for the mitigation of membrane fouling in a membrane bioreactor, Sep. Purifi. Technol. 159 (2016) 124-134. https://doi.org/10.1016/j.seppur.2016.01.003.

[14] W. Sohn, W. Guo, H.H. Ngo, L. Deng, D. Cheng, X. Zhang, A review on membrane fouling control in

anaerobic membrane bioreactors by adding performance enhancers, J. Water Process Eng. 40 (2021) 101867. https://doi.org/10.1016/j.jwpe.2020.101867.

[15] S. Khan, M. Naushad, A. Al-Gheethi, J. Iqbal, Engineered nanoparticles for removal of pollutants from wastewater: Current status and future prospects of nanotechnology for remediation strategies, J. Environ. Chem. Eng. 9(5) (2021). https://doi.org/10.1016/j.jece.2021.106160.

[16] N. Wang, X. Li, Y.L. Yang, Z.W. Zhou, Y. Shang, X.X. Zhuang, Photocatalysis-coagulation to control ultrafiltration membrane fouling caused by natural organic matter, J. Clean. Prod. 265 (2020). https://doi.org/10.1016/j.jclepro.2020.121790.

[17] Y. Gao, D. Ma, Q. Yue, B. Gao, X. Huang, Effect of powdered activated carbon (PAC) on MBR performance and effluent trihalomethane formation: At the initial stage of PAC addition, Bioresour. Technol. 216 (2016) 838-44. https://doi.org/10.1016/j.biortech.2016.06.030.

[18] J.W. Wang, A. Cahyadi, B. Wu, W. Pee, A.G. Fane, J.W. Chew, The roles of particles in enhancing membrane filtration: A review, J. Membr. Sci. 595 (2020). https://doi.org/10.1016/j.memsci.2019.117570.

[19] L. Deng, W. Guo, H.H. Ngo, H. Zhang, J. Wang, J. Li, S. Xia, Y. Wu, Biofouling and control approaches in membrane bioreactors, Bioresour. Technol. 221 (2016) 656-665. https://doi.org/10.1016/j.biortech.2016.09.105.

[20] T. Zhou, Y. Wang, T. Li, H. Li, C. Yang, D. Sun, D. Wang, C. Liu, G. Che, Fabricating magnetic hydrophilic molecularly imprinted resin with enhanced adsorption and recognition performance for targeted detecting chlorophenols in environmental water, Chem. Eng. J. 420 (2021) 129904. https://doi.org/10.1016/j.cej.2021.129904.

[21] J. Yao, Y. Ma, J. Liu, S. Liu, J. Pan, Janus-like boronate affinity magnetic molecularly imprinted nanobottles for specific adsorption and fast separation of luteolin, Chem. Eng. J. 356 (2019) 436-444. https://doi.org/10.1016/j.cej.2018.09.003.

[22] S. Farooq, H.Y. Wu, J.Y. Nie, S. Ahmad, I. Muhammad, M. Zeeshan, R. Khan, M. Asim, Application, advancement and green aspects of magnetic molecularly imprinted polymers in pesticide residue detection, Sci. Total Environ. 804 (2022). https://doi.org/10.1016/j.scitotenv.2021.150293.

[23] H. Guo, J. Hu, J. Li, M.-t. Gao, Q. Wang, W. Guo, H.H. Ngo, Systematic insight into the short-term and long-term effects of magnetic microparticles and nanoparticles on critical flux in membrane bioreactors, J. Membr. Sci. 582 (2019) 284-288. https://doi.org/10.1016/j.memsci.2019.04.015.

[24] Y. Liu, J. Li, W. Guo, H.H. Ngo, J. Hu, M.-t. Gao, Use of magnetic powder to effectively improve the performance of sequencing batch reactors (SBRs) in municipal wastewater treatment, Bioresour. Technol. 248 (2018) 135-139. https://doi.org/10.1016/j.biortech.2017.06.069.

[25] P. Zahedi, M. Ziaee, M. Abdouss, A. Farazin, B. Mizaikoff, Biomacromolecule template-based molecularly imprinted polymers with an emphasis on their synthesis strategies: a review, Polym. Adv. Technol. 27 (9) (2016) 1124-1142. https://doi.org/10.1002/pat.3754.

[26] M. Dinc, C. Esen, B. Mizaikoff, Recent advances on core–shell magnetic molecularly imprinted polymers for biomacromolecules, TrAC Trends Anal. Chem. 114 (2019) 202-217. https://doi.org/10.1016/j.trac.2019.03.008.

[27] K. Poojamnong, K. Tungsudjawong, W. Khongnakorn, P. Jutaporn, Characterization of reversible and irreversible foulants in membrane bioreactor (MBR) for eucalyptus pulp and paper mill wastewater treatment using fluorescence regional integration, J. Environ. Chem. Eng. 8(5) (2020). https://doi.org/10.1016/j.jece.2020.104231.

[28] D.Q. Zhang, A.P. Trzcinski, C. Kunacheva, D.C. Stuckey, Y. Liu, S.K. Tan, W.J. Ng, Characterization of soluble microbial products (SMPs) in a membrane bioreactor (MBR) treating synthetic wastewater containing pharmaceutical compounds, Water Res. 102 (2016) 594-606.

https://doi.org/10.1016/j.watres.2016.06.059.

[29] R. Xing, S. Wang, Z. Bie, H. He, Z. Liu, Preparation of molecularly imprinted polymers specific to glycoproteins, glycans and monosaccharides via boronate affinity controllable-oriented surface imprinting, Nat. Protoc. 12 (5) (2017) 964-987. https://doi.org/10.1038/nprot.2017.015.

[30] Q. Wu, M. Li, Z. Huang, Y. Shao, L. Bai, L. Zhou, Well-defined nanostructured core-shell magnetic surface imprinted polymers (Fe_3O_4@SiO_2@MIPs) for effective extraction of trace tetrabromobisphenol A from water, J. Ind. Eng. Chem. 60 (2018) 268-278. https://doi.org/10.1016/j.jiec.2017.11.013.

[31] Y. Liu, Q. Liu, J. Li, H.H. Ngo, W. Guo, J. Hu, M.T. Gao, Q. Wang, Y. Hou, Effect of magnetic powder on membrane fouling mitigation and microbial community/composition in membrane bioreactors (MBRs) for municipal wastewater treatment, Bioresour. Technol. 249 (2018) 377-385. https://doi.org/10.1016/j.biortech.2017.10.027.

[32] Y.J. Zhu, L.J. Cao, Y.Y. Wang, Characteristics of a Self-Forming Dynamic Membrane Coupled with a Bioreactor in Application of Anammox Processes, Environ. Sci. Technol. 53(22) (2019) 13158-13167. https://doi.org/10.1021/acs.est.9b04314.

[33] E.A. Dil, A.H. Doustimotlagh, H. Javadian, A. Asfaram, M. Ghaedi, Nano-sized Fe_3O_4@SiO_2-molecular imprinted polymer as a sorbent for dispersive solid-phase microextraction of melatonin in the methanolic extract of Portulaca oleracea, biological, and water samples, Talanta 221 (2021). https://doi.org/10.1016/j.talanta.2020.121620.

[34] J. Miao, X.J. Zhao, Y.X. Zhang, Z.H. Liu, Feasible synthesis of hierarchical porous MgAl-borate LDHs functionalized Fe3O4@SiO2 magnetic microspheres with excellent adsorption performance toward congo red and Cr(VI) pollutants, J. Alloy. Compd. 861 (2021). https://doi.org/10.1016/j.jallcom.2020.157974.

[35] H.L. Jiang, Y. Cao, F.T. Zeng, Z.W. Xie, F. He, A Novel Fe_3O_4/Graphene Oxide Composite Prepared by Click Chemistry for High-Efficiency Removal of Congo Red from Water, J. Nanomater 2021 (2021). https://doi.org/10.1155/2021/9716897.

[36] J.Q. Xu, Q. Zhang, F. Guo, J.P. Hong, W. Chu, Effects of the crystallization time on the mesoporous structure, texture, morphology and styrene oxidation performances of V-MCM-41, J. Energy. Chem. 25(6) (2016) 1058-1063. https://doi.org/10.1016/j.jechem.2016.10.004.

[37] Y. Feng, G. Wei, Y. Liu, W. Han, Y. Chen, R. Sun, L. Peng, M. Ma, Y. Zhang, Z. Zhang, X. Lu, Crystallization behavior of boron in low-temperature immobilization of iodine waste, J. Solid. State. Chem. 305 (2022). https://doi.org/10.1016/j.jssc.2021.122698.

[38] X.J. Li, B.L. Zhang, W. Li, X.F. Lei, X.L. Fan, L. Tian, H.P. Zhang, Q.Y. Zhang, Preparation and characterization of bovine serum albumin surface-imprinted thermosensitive magnetic polymer microsphere and its application for protein recognition, Biosens. Bioelectron. 51 (2014) 261-267. https://doi.org/10.1016/j.bios.2013.07.008.

[39] G. Su, L.H. Liu, L.X. Zhang, X. Liu, J.R. Xue, A.P. Tang, Fabrication of magnetic Fe_3O_4@SiO_2@$Bi_2O_2CO_3$/rGO composite for enhancing its photocatalytic performance for organic dyes and recyclability, Environ. Sci. Pollut. R. 28(36) (2021) 50286-50301. https://doi.org/10.1007/s11356-021-14248-z.

[40] Y. Cao, T. Sheng, Z. Yang, D. Huang, L. Sheng, Synthesis of molecular-imprinting polymer coated magnetic nanocomposites for selective capture and fast removal of environmental tricyclic analogs, Chem. Eng. J. 426 (2021) 128678. https://doi.org/10.1016/j.cej.2021.128678.

[41] H.P. Zeng, L.X. Zhai, T.D. Qiao, Y.P. Yu, J. Zhang, D. Li, Efficient removal of As(V) from aqueous media by magnetic nanoparticles prepared with Iron-containing water treatment residuals, Sci. Rep-UK. 10(1) (2020). https://doi.org/10.1038/s41598-020-65840-1.

[42] Z. Liu, H. He, Synthesis and Applications of Boronate Affinity Materials: From Class Selectivity to

Biomimetic Specificity, Acc. Chem. Res. 50 (9) (2017) 2185-2193. https://doi.org/10.1021/acs.accounts.7b00179.

[43] D.J. Li, Y. Chen, Z. Liu, Boronate affinity materials for separation and molecular recognition: structure, properties and applications, Chem. Soc. Rev. 44(22) (2015) 8097-8123. https://doi.org/10.1039/c5cs00013k.

[44] R. Gao, Y. Hao, L. Zhang, X. Cui, D. Liu, M. Zhang, Y. Tang, Y. Zheng, A facile method for protein imprinting on directly carboxyl-functionalized magnetic nanoparticles using non-covalent template immobilization strategy, Chem. Eng. J. 284 (2016) 139-148. https://doi.org/10.1016/j.cej.2015.08.123.

[45] J.X. Li, B.Q. Jiang, Y. Liu, C.Q. Qiu, J.J. Hu, G.R. Qian, W.S. Guo, H.H. Ngo, Preparation and adsorption properties of magnetic chitosan composite adsorbent for Cu^{2+} removal, J. Clean. Prod. 158 (2017) 51-58. https://doi.org/10.1016/j.jclepro.2017.04.156.

[46] Y.Y. Xu, Q.F. Dang, C.S. Liu, J.Q. Yan, B. Fan, J.P. Cai, J.J. Li, Preparation and characterization of carboxyl-functionalized chitosan magnetic microspheres and submicrospheres for Pb^{2+} removal, Colloid Surf. A 482 (2015) 353-364. https://doi.org/10.1016/j.colsurfa.2015.06.028.

[47] J. Luo, S. Jiang, X. Liu, Efficient One-Pot Synthesis of Mussel-Inspired Molecularly Imprinted Polymer Coated Graphene for Protein-Specific Recognition and Fast Separation, J. Phys. Chem. C 117 (36) (2013) 18448-18456. https://doi.org/10.1021/jp405171w.